Article

Preliminary Evaluation of a Numerical System of Prediction for Surface Solar Irradiance and Cloudiness in a Site with a Subtropical Humid Climate.

Gabriel Cazes Boezio [1,†,‡]

[1] Universidad de la República, Facultad de Ingeniería, IMFIA; agcm@fing.edu.uy
* Correspondence: agcm@fing.edu.uy;
† Current address: J. Herrera y Reissig 565, Montevideo Uruguay. cp11300.

Abstract: This study explores a prediction system for global horizontal irradiance and cloudiness in a humid subtropical terrestrial region. This system consists of regional simulations performed with the Weather Research and Forecasting model using the initial and boundary conditions from the Global Forecast System. The predictions show significant biases for the variable of interest, with notable variations within the daily and annual cycles. The study also finds significant biases in cloud incidence and clarity index predictions, with relevant diurnal and seasonal variations. During austral summer, multiplying the relative humidity of initial and boundary conditions by a fixed factor improves the forecasts of global horizontal irradiance and cloud incidence for the central hours of the day and the afternoon. During austral winter, an empirical correction of the clarity index obtained from the simulation's outputs also shows the potential to improve the forecasts' biases. This work proposes a hypothesis about the causes of the forecast biases.

Keywords: Weather Research and Forecast Model; cloud prediction; humid climate; forecast biases; empirical corrections

1. Introduction

Predicting surface irradiance is important in managing large-scale photovoltaic systems, though it can be limited by the poor prediction of cloudiness in humid regions. This study investigates the accuracy of a numerical prediction system for global horizontal irradiance (GHI) at a location in central Uruguay within southeastern South America (SESA).

The relative importance of specific physical processes related to clouds may differ in each region and even in different seasons, which can affect the performance of any given forecast system for GHI. Besides this, the performance of numerical predictions also depends on the availability of data to initialize the numerical simulations, which differ among various regions. Therefore, the conclusions for a specific area are not directly applicable to others. There are several published works about numerical predictions of GHI in humid climates, but very few in SESA. As examples of works of this kind in other humid climates, we can refer to the works by Mathiesen and Kleis (2011) [1], Huang and Thatcher (2017) [2], and Bezerra et al. (2024) [3]. In southeastern South America, Rincón et al. (2018) [4] studied a system of model output statistics to correct numerical simulations of GHI in Paraguay, obtained from the WRF model with initial and boundary conditions obtained from NCEP reanalysis (the simulations were in analysis rather than in forecast mode). The authors considered ground measurements of GHI during 2015 and found that the simulations had significant biases. The uncorrected simulations showed relative bias between 10 and 15 percent during winter and fall and between 20 and 25 % during spring and summer. The relative root mean square errors were, on average, more than 70%. The systems of model output statistics employed reduced the relative bias to values below 5%

Citation: Lastname, F.; Lastname, F.; Lastname, F. Title. *Journal Not Specified* **2024**, *1*, 0. https://doi.org/

Received:
Revised:
Accepted:
Published:

and relative RMSE to values from 40 to 60%. Texeira Branco et al. (2022) [5] evaluated GHI forecasts for the first 24 hours in Uruguay, obtained from a NOAA Global Forecast System forecast, comparing them with data from several ground stations available for this study for three years from 2017 to 2019. Their study found a systematic overestimation of GHI, from 3.5% in the central and late hours of the day to 15% during the early hours. However, this study did not show the seasonal cycle of these errors or discuss the compensation of errors during different seasons.

The present work explores a specific numerical system for GHI prediction in Uruguay for time horizons within 24 hours. It emphasizes determining the seasonal and daily cycles of the predictions' systematic errors and proposing techniques to alleviate such systematic errors. The methodologies described can be a base for developing an optimized forecast system, although such optimization is beyond the scope of this work. This work also proposes a hypothesis about some of the causes of bias.

Next, we describe the main characteristics of the climate in SESA, especially those aspects associated with clouds, and we point out the numerical predictability of these processes.

SESA is a subtropical region with a humid climate and an average annual precipitation of 1000–1500 mm/year, without a particularly distinct seasonal cycle (Ferreira and Reboita, 2022[6]). It is affected by cyclogenesis processes and the associated frontal developments throughout the year (Gan and Rao 1991 [7], Rao et al. 2002 [8], Vera et al. 2002 [9]). The development of deep convection is also important. It can be associated with frontal processes (Ross and Orlanski, 1978[10], Rassmusen et al. 2016 [11], Siqueira and Machado 2004 [12]) and also with mesoscale convective complexes (MCCs), which are of great importance in the region (Velasco and Fritsch 1987 [13], Salio et al. 2007 [14]). The predictability of baroclinic processes and MCCs is substantial, with numerous studies demonstrating skillful forecasts within 24-hour lead times (Seluski and Saulo 1998 [15], Satyamurti and Bittencourt 1999 [16], Ortelli 2023 [17]). Orteli (2023) [17] analyzed the quality of precipitation predictions obtained from the ensemble forecasts of the United States National Ocean and Atmosphere Administration (NOAA)'s Global Forecast System (GFS) and from the European Centre for Medium-Range Weather Forecasts in a subregion of Uruguay. Their study found significant prediction abilities for both systems within horizons of up to 5 days. The prediction capacity is confirmed for both frontal processes and MCCs. These results suggest that the incidence of clouds related to these processes has good potential for numerical predictability in the region and within the 24-hour temporal horizon considered in this work. These clouds are generally thick, and their tops occur in the middle or upper troposphere.

The region of interest is also affected by low-level cloudiness, including stratocumulus and shallow cumulus clouds. These cloud types are related to shallow convection processes and are affected by the characteristics of the atmospheric boundary layer (ABL). Porrini (2017) [18] studied the 24-hour predictability of solar irradiance at various locations in Uruguay during the austral summer using a forecast system similar to that used here and found that, during the central hours of the day, there was an overestimation of the frequency of clear-sky days, partly attributable to a systematic underestimation of low-level cloudiness. Therefore, cloud prediction should consider synoptic and mesoscale processes as well as cloud development related to shallow convection processes. The predictability of clouds related to synoptic and mesoscale processes is high in the region of interest, whereas the forecasting of low-level clouds directly related to atmospheric boundary layer processes and shallow convection remains challenging.

In recent years, there have been considerable advances in the numerical modeling of ABL processes, several of which have been incorporated into the ABL parameterizations available in the Weather Research Forecasting (WRF) model (Skamarock et al. 2017) [19], including the Yon Sei University ABL scheme (Hong et al. 2009) [20] and the Washington University ABL scheme (Bretherton et al. 2004) [21]. Both schemes effectively reproduce marine stratocumulus clouds in the tropical eastern Pacific. Marine stratocumulus clouds are also well simulated by the ABL schemes described by Konor et al. (2009) [22] and Lock (1998) [23]. The predictability of shallow cumulus clouds has also been improved through numerical schemes described by Park and Bretherton (2009) [24], Grell (1993) [25], and Kain and Fritch (1993) [26]. Despite these advances, the predictability of stratocumulus and shallow cumulus clouds can vary in different climates or depend on specific simulation systems.

The objectives of this study are as follows:

- To evaluate primarily the GHI predictions at the study site within a 24-hour horizon. The prediction system consists of regional simulations obtained from the WRF model (Scamarok et al., 2017) [19] with initial and boundary conditions prescribed by the GFS system.
- To evaluate the predictions of clouds with different ranges of cloud-top heights at the study site.
- To evaluate the sensitivity of the GHI and cloudiness predictions to specific initial and boundary condition modifications.

2. Data Used and Numerical Experiments

2.1. Global Horizontal irradiance filed data

This work uses GHI measurements from a pyranometer that belongs to a meteorological station at the Bonete hydropower plant, located approximately in the middle of Uruguay (see Fig. 1). The station is part of a network that measures wind velocity at heights up to 100 m above the ground and solar radiation near the ground, operated by the National Administration of Electric Power Plants and Transmissions of Uruguay (Usinas y Trasmisiones del Estado; UTE) since 2008. This network is described by Cornalino and Draper (2012) [27], and its measurements (including GHI averaged every 10 min) are made available online by UTE.

2.2. Numerical Simulations

The regional simulations take their initial and boundary conditions from global predictions made by the GFS. The horizontal grid of the regional simulations has a resolution of 0.25° in the zonal and meridional directions. It has 49 grid points in both directions and is centered at the location of Bonete station (Fig. 1).

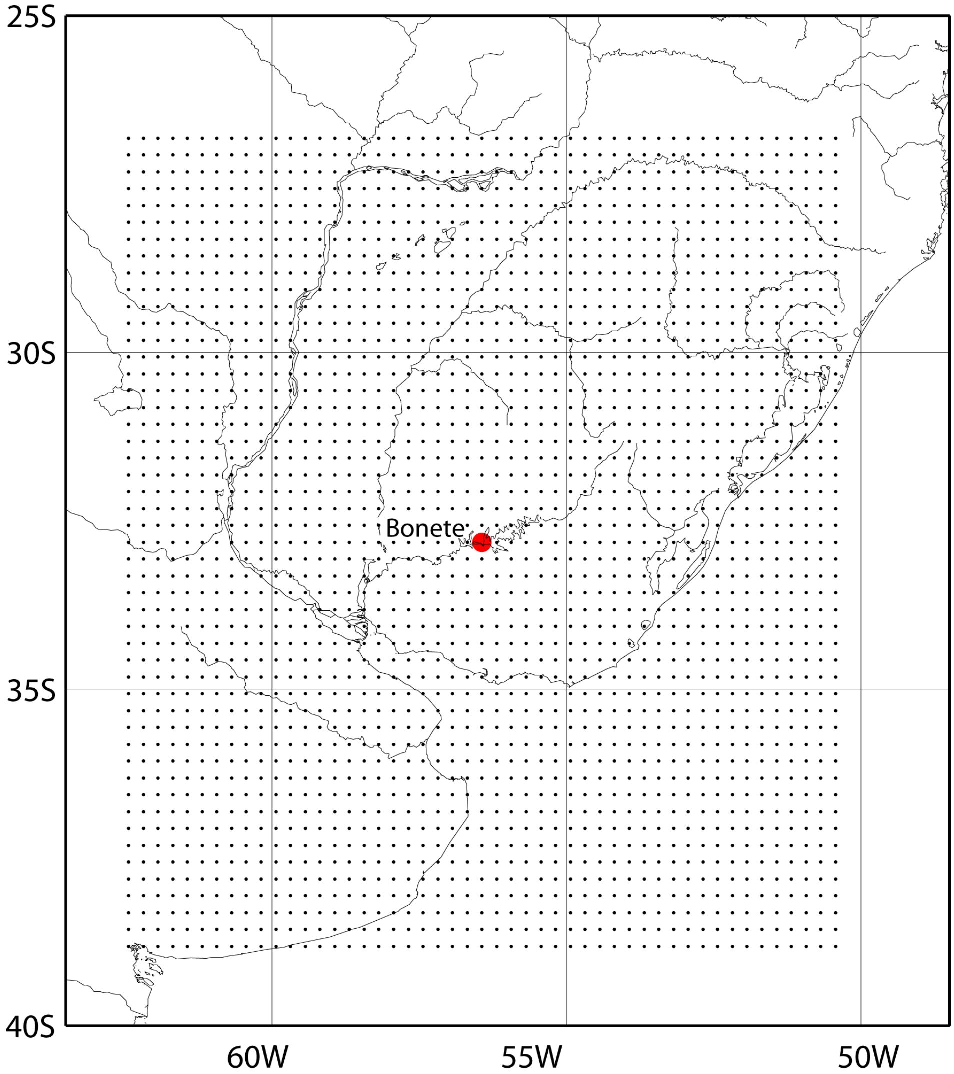

Figure 1. Grid points of the horizontal discretization used in the regional simulation. The larger red point indicates the location of Bonete station.

Appendix A shows the vertical discretization used. It has 33 layers; the highest vertical resolution is concentrated in the first three thousand meters. Over Bonete, the thickness of the first 20 layers above the terrain is around 150 meters. The choice of such a high resolution in the lower troposphere was made with the aim of improving the simulation of processes related to shallow convection.
The set of reference simulations extends 24 hours and starts at 0:00GMT daily from November 1st 2018 to October 31st 2023. The parameterizations of physical processes used in the reference simulations are listed in Appendix A.

2.2.1. Modification of Initial and Boundary Conditions

Some simulations in this work modify the water content of the initial and boundary conditions derived from the GFS data. A multiplying factor, called WPS, affects the relative humidity field (RH) that is included in the output files of the WRF preprocessing module. The WPS module, described by Sclamarock et al. (2017)[19], horizontally interpolates meteorological data onto the horizontal grid of the projected domain at the time slices selected to prescribe initial and boundary conditions to the regional simulation. The results of the WPS module are the "met" files, which are used as input to a specific program (real.exe) that completes the build of the files for initial and boundary conditions. The "met" files contain surface and 3-dimensional fields of temperature, total water content in terms of relative humidity (RH variable), geopotential height, pressure, and the horizontal components of wind speed, as well as the 2-dimensional fields of static terrestrial properties. The water content used to build the initial and boundary conditions is modified as follows: the RH variable is read from the "met" files, multiplied by a uniform factor at all the vertical levels of the "met" files, and re-written to the "met" files. Appendix A shows a scheme of this procedure.

2.2.2. Clear-sky simulations and clarity index (K_c)

To define GHI for clear sky conditions, we perform simulations for the whole period with the WRF model in the conditions described above, except that inside the short-wave radiation routine, we set the water content of clouds in their liquid, ice, and rain phases to zero.

For any given prediction of GHI in any WRF configuration, we define the clarity index (K_c) as

$$K_{cpredicted} = (predicted\ GHI)/(clear\ sky\ GHI) \tag{1}$$

where the predicted and the clear-sky GHI correspond to the same instant.

Analogously, for any given measurement of GHI at the pyranometer of Bonete station, the observed K_c is

$$K_{cmeasured} = (measured\ GHI)/(clear\ sky\ GHI). \tag{2}$$

Again, the observation and the clear-sky prediction correspond to the same instant.

2.3. Cloud incidence and cloud top height data from MODIS satellites

This work considers cloud incidence and cloud top height based on analysis of measurements obtained by MODIS Terra and Aqua satellites, which are made available by NASA's Level-1 and Atmosphere Archive Distribution System (NASA LAADS DAAC). Cloud incidence is taken from MODIS Cloud Mask Products, and cloud top heights are taken from MODIS Cloud Products (Platnick et al., 2015 [28]; King et al., 2003 [29]). Figure 2 shows histograms of the frequency of overpasses through Bonete of the Terra and Aqua satellites as a function of local time (UTC minus 3 hours). The Terra satellite provides information at this site late in the morning and noon, while the Aqua satellite provides information in the early afternoon.

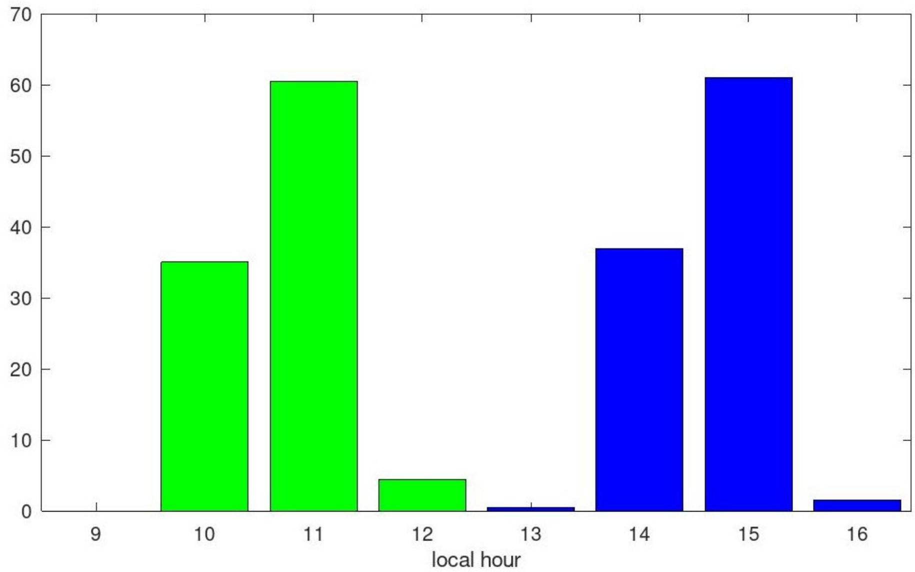

Figure 2. Histogram of the frequencies at which the MODIS Terra satellite (green bars) and the MODIS Aqua satellite (blue bars) overpass Bonete for time intervals of the local hour.

2.3.1. Mean cloud incidences

The mean incidence of clouds at a specific time of day and during a particular season is defined for both forecasts and MODIS analysis results as

$$i = \frac{Y}{n} \tag{3}$$

where Y is the number of instances in which forecasts or the MODIS analysis detects clouds over Bonete and n is the total number of days within the season of interest between November 2018 and October 2023. We calculate forecasted and MODIS-diagnosed average incidences when the Terra and Aqua satellites overpass Bonete.

For the forecasts, clouds are considered to be detected if the specific content of cloud liquid water or cloud ice is greater than zero at some point in the vertical grid at the horizontal grid point that corresponds to the Bonete site. Note that cloud detection by MODIS analysis and numerical forecasts are defined differently. The MODIS analysis considers specific properties of radiation measured by the Terra and Aqua satellites (King et al. (2003) [29], Platnick et al. (2021) [30]), but not all of these properties are readily available from the numerical simulations used for the forecasts. On the other hand, water content is available from the simulations but not directly measured by the satellites. Therefore, cloud incidences obtained from MODIS analysis may be considered as a qualitative reference for forecasted cloud incidences, while it is possible to make direct quantitative comparisons between the cloud incidences obtained from different kinds of numerical simulations used in this work.

2.4. GHI data from NASA POWER analysis

To complement the field data of the Bonete station, we consider GHI estimates from the National Aeronautics and Space Administration (NASA) Langley Research Center (LaRC) Prediction of Worldwide Energy Resource (POWER) Project funded through the NASA Earth Science/Applied Science Program (NASA POWER analysis). This database estimates solar radiation from satellite observations and meteorological data from assimilation models and is described by Lauret et al. (2017) [31].

2.5. Forecast metrics and statistical significances

2.5.1. Relative bias (RBIAS) and RRMSE

If a is the GHI measured at a given hour during a particular month or season and b is the correspondent prediction, the relative bias (RBIAS) is defined as

$$rbias = \frac{\overline{(b\ -\ a)}}{\overline{a}} \tag{4}$$

where the overline indicates the average over all the cases within the month or season considered.

The relative root mean square error (RRMSE) is defined as

$$rrmse = \frac{\sqrt{\overline{(b\ -\ a)^2}}}{\overline{a}} \tag{5}$$

2.5.2. Statistical significance for biases and differences of mean cloud incidences

Because biases are differences in means, it is possible to compute their significance with a two-tailed Student t-test as described by Press et al. (1992) **??**. The same test is applied to the differences in bias.

The statistical significances of differences in mean cloud incidences between forecasts and MODIS analysis or between different types of forecasts were computed as indicated by Snedeckor and Cochran (1967) [34]. We define the variable z as

$$z = \frac{i_1 - i_2}{\sqrt{i(1-i)(\frac{1}{n_1} + \frac{1}{n_2})}} \tag{6}$$

where i_1 and i_2 are the average incidences to be compared and n_1 and n_2 are the total number of days within the samples. The parameter i is computed as

$$i = \frac{Y_1 + Y_2}{n_1 + n_2} \tag{7}$$

In our cases, n_1 and n_2 are equal and correspond to the total number of days within the season of interest from November 2018 to October 2023. The differences are considered statistically significant at the 5% level when the value of z corresponds to a percentile below 0.025 or above 0.975 of a normal distribution with an expected value of zero and a unit standard deviation.

3. Results

We assess the availability of solar resources at Bonete based on the average monthly GHI from November 2018 to October 2023 at 10:00, 12:00, 14:00, and 16:00 local time (Fig. 3a), along with the corresponding average of measured K_c indices (Fig. 3b). We find that the K_c indices have moderate-amplitude daily and annual cycles.

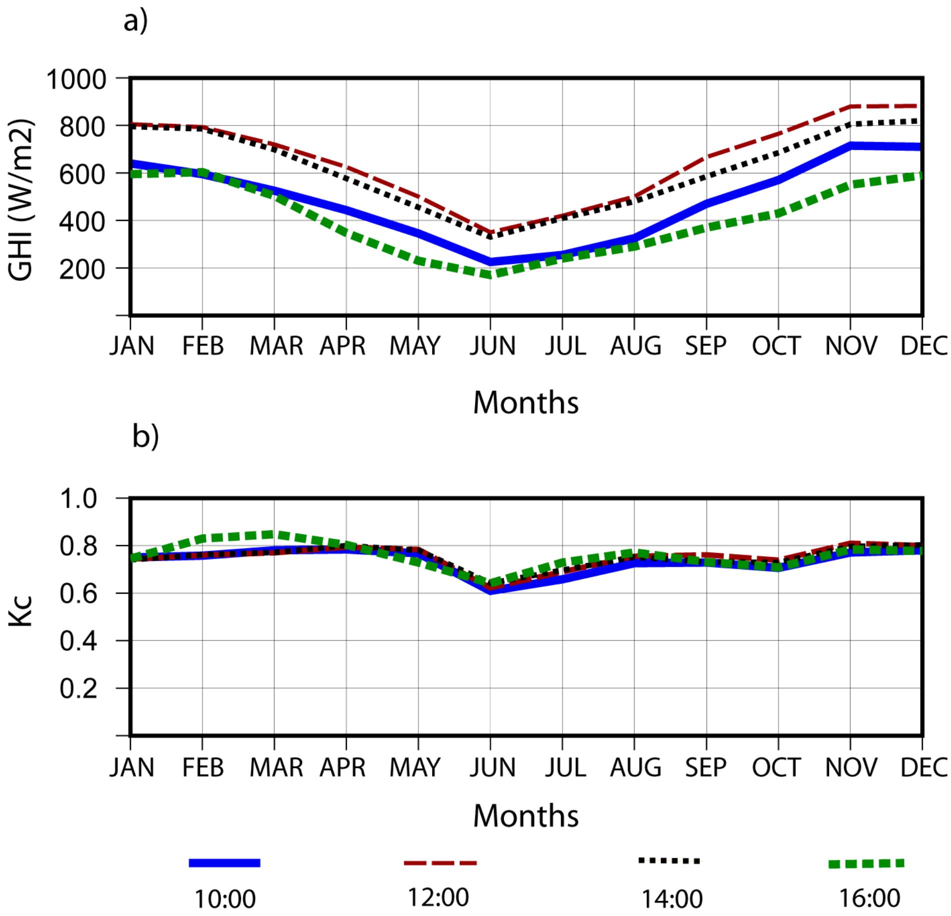

Figure 3. (a) Observed monthly means of GHI at Bonete for local times of 10:00, 12:00, 14:00 and 16:00. (b) Monthly means of measured K_c indices for the same local times considered in (a).

Figure 4 shows the relative biases in the GHI reference predictions compared to the field measurements for each month at the times of the day considered in Fig. 3. There are important differences between summer and winter. In the austral summer (DJF), we find positive biases at 10:00 and, to a greater extent, at 12:00, 14:00, and 16:00. During the austral winter (JJA), we find pronounced negative biases at 10:00 and, to a lesser extent, at 12:00 and 16:00.

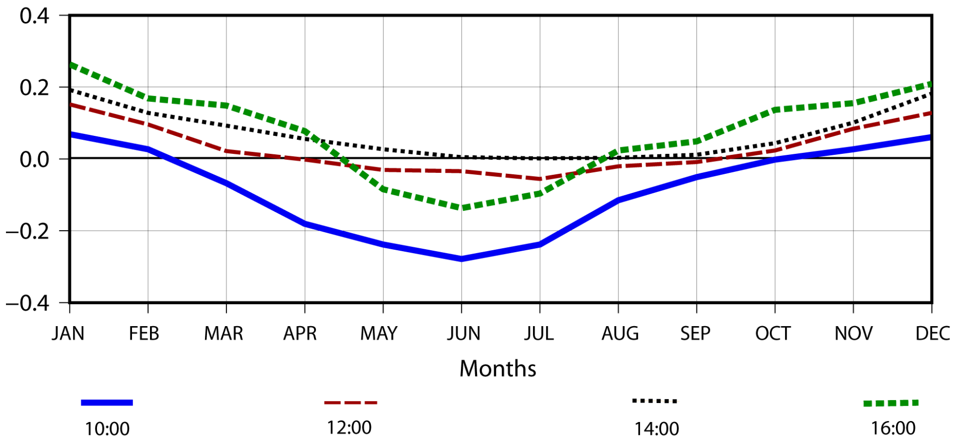

Figure 4. Relative bias for the reference forecast of GHI at Bonete for each month at 10:00, 12:00, 14:00, and 16:00, local time.

As a complement to this information, Fig. 5 shows the relative bias of GHI forecasts for each local hour from 10:00 to 16:00 for the bimesters January–February, March–April, May–June, July–August, September–October, and November–December. During the November–December and January–February bimesters, the forecasts underestimated GHI in the early morning and overestimated it at noon and in the afternoon. During the May–June and July–August bimesters, the relative bias is reduced during the central hours but is significantly negative in the early morning and late afternoon.

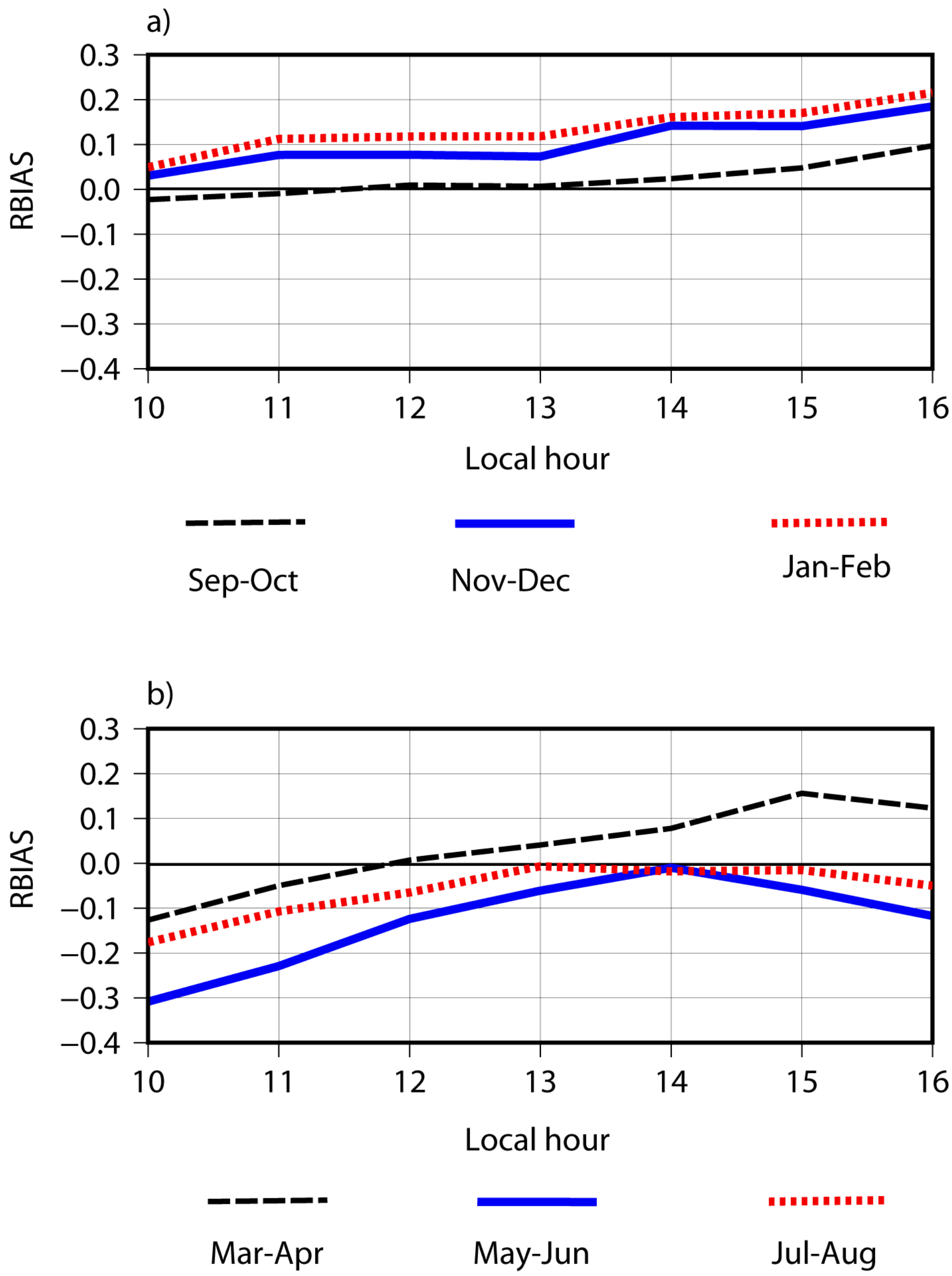

Figure 5. Relative bias for the reference forecast of GHI at Bonete as a function of local time, from 10:00 to 16:00. (a) September–October, November–December, and January–February bimesters. (b) March–April, May–June, and July–August bimesters.

Significant biases in a deterministic prediction system imply systematic errors in one or more components and limit the system's performance in practice. Considering the seasonality of the biases, we focus on the periods between November and February (NDJF), which shows the most considerable positive biases during the central and afternoon hours, and between May and August (MJJA), which exhibits the most significant negative bias in the morning. Although there is some level of arbitrariness in the choice of these seasons, they allow us to sample the seasonal cycle in seasons that show essential differences in terms of the systematic errors of the forecasts.

We analyze the prediction biases and other performance metrics of GHI forecasts throughout the day during these seasons, along with the incidence of predicted clouds, averaged according to the pass times of the Terra and Aqua satellites, and compare these values with the corresponding MODIS analyses.

3.1. The NDJF season

Several WRF parameterizations, including the WRF-Solar model, were tested to improve predictions, but all underestimated cloud incidence and overestimated GHI during the central hours of the day and the afternoon. However, two alternative methodologies improved the systematic deviations of the predictions without compromising the other forecast metrics considered.

- The initial and boundary conditions of the simulations were modified by systematically increasing RH by a factor of 1.2. Although this is a simple modification (independent of the vertical level and geographic location), it allows for a preliminary exploration of predictions' sensitivity to changes in this variable.
- We tested forecasts that used the Yonsei University ABL scheme (Hong et al. 2006**??**) and an increased RH of the initial and boundary conditions as explained above (YSUBL-RHx1.2 simulations); forecasts that used the Washington University ABL scheme (Bretherton et al. 2004**??**) with the same modification of initial and boundary conditions (WUBL-RHx1.2); and a composite forecast that considered for each hour the forecast among these two that produced the lowest GHI value. These predictions were called COMP.

Figure 6 shows the relative biases in the reference, YSUBL-RHx1.2, WUBL-RHx1.2, and COMP predictions for NDJF between 8:00 and 18:00 local time during the years 2018–2019 and 2022–2023. The reference forecasts show a sizable negative bias at 8:00, which evolves into a strong positive bias exceeding 10% from 11:00 onward. These biases are statistically significant at a 5% level at each round hour. Between 8:00 and 10:00, the YSUBL-RXx1,2, WUBL-RHx1.2, and COMP forecasts have negative biases worse than those of the reference forecast, while the new ones improve the positive biases of the reference forecasts from 12:00 onward. The COMP forecast bias improves the YSUBL-RHx1.2 and UWBL-RHx1.2 forecasts from 16:00 to 18:00. As for the statistical significance of these differences, the biases of the YSUBL-RHx1.2, UWABL-RHx1.2, and COMP forecasts are different from the bias of the reference forecasts, with statistical significance at a 5% level from 8:00 to 18:00. In addition, the bias of the COMP forecasts is different from the biases of both the YSUBL-RHx1.2 and UWABL-RHx1.2 forecasts, with statistical significance at a 5% level from 16:00 to 18:00.

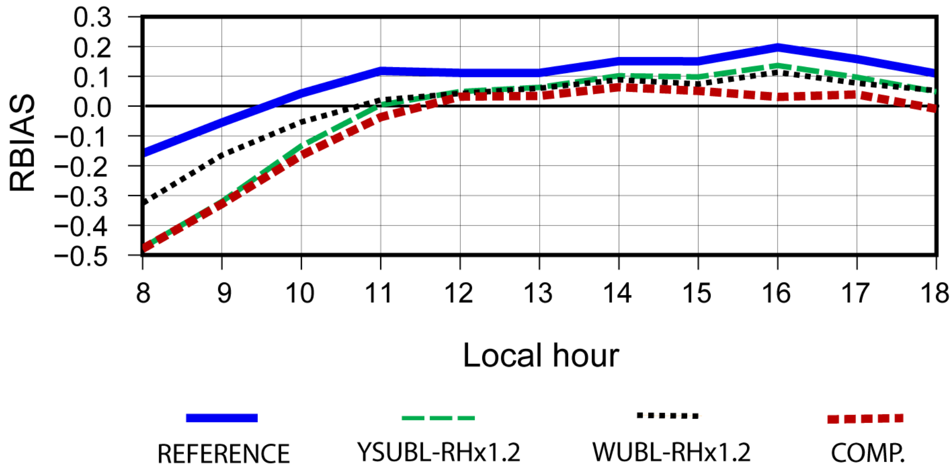

Figure 6. Relative bias of GHI forecasted at Bonete during the NDJF season, as a function of local time. Black, reference forecast; blue, YSUBL-RHx1.2 forecast; magenta, WUBL-RHx1,2 forecast; red, COMP forecast.

The biases found for the reference forecast indicate errors in predicting the incidence or thickness of clouds. However, based only on the information from the simulations, we cannot deduce the relative importance of these factors or whether they are concentrated in specific altitude ranges. We compare the simulation results with cloud information derived from MODIS Terra and Aqua satellite data to gain insights.

Table 1 indicates the percentage of days within these seasons when clouds are predicted at the passing times of the Terra satellite by the four schemes considered in Fig. 6 and the corresponding percentage when the MODIS analysis indicates the presence of clouds. It also considers subpopulations of clouds with tops above and below 3000 m to distinguish between mid/high and low clouds. For the reference forecasts, the mean predicted cloud incidence is smaller than the corresponding MODIS analysis in all categories by 10-15%, with these differences being statistically significant to a 5% level (according to the test described in Section 2). The YSUBL-RHx1.2, WUBL-RHx1.2, and COMP forecasts increase cloud incidences in all categories, reaching values similar to those from MODIS analysis.

Table 1. Cloud incidences at times when the Terra satellite overpasses Bonete during NDJF, forecasted by the reference, YSUBL-RHx1.2, WUBL-RHx1.2, and COMP predictions and diagnosed by MODIS.

Cloud incidences at times of MODIS Terra overpasses			
	All clouds	**Clouds tops > 3000m**	**Cloud tops < 3000m**
Reference forecasts	24.8	19.7	5.0
YSUBL-RHx1.2 forecasts	40.1	25.0	15.1
WUBL-RHx1.2 forecasts	39.4	26.6	12.8
COMP forecasts	45.3	26.4	18.9
Diagnosed by MODIS	40.9	27.7	13.2

The first column of Table 2 shows the mean predicted K_c index for cases when predictions indicate clouds at times that the Terra satellite overpasses Bonete (first to fourth rows) and the mean measured K_c index for cases when the Terra satellite effectively detects clouds (fifth row). The second and third columns are analogous to the first for clouds with tops >3000 m (second column) or <3000 m (third column). The predicted and measured K_c indices are similar on average for the reference forecasts. The predictions have more clarity in high-cloud cases and less in low-cloud cases. The YSU-RHx1.2, WU-RHx1.2, and COMP predictions have a mean K_c slightly lower than reference predictions and measures.

Table 2. Mean K_c indexes at times when the Terra satellite overpasses Bonete. The first row shows mean K_c indexes from reference predictions when these predictions determined clouds over Bonete at times of Terra overpasses. The second, third, and fourth rows are analogous to the YSUBL-RHx1.2, WUBL-RHx1.2, and COMP predictions. The fifth row shows the mean measured K_c indexes when MODIS analysis detected clouds at times of Terra overpasses Bonete.

K_c **index at times of Terra overpasses**			
	All clouds	**Clouds tops > 3000m**	**Cloud tops < 3000m**
K_c form reference forecasts	.54	.55	.50
K_c from YSUBL-RHx1.2 forecasts	.50	.48	.53
K_c from WUBL-RHx1.2 forecasts	.51	.47	.59
K_c from COMP forecasts	.49	.46	.52
K_c from measurements	.56	.49	.72

Tables 3 and 4 are analogous to Tables 1 and 2 but refer to the Aqua satellite data. The reference predictions have lower mean cloudiness than MODIS analysis in all the categories, with magnitudes similar to those for the Terra satellite (Table 3). The differences are statistically significant to a level of 5%. In addition, the average clarity from the reference forecasts for predicted cloudy cases is higher than that for measured cloudy cases for all categories. The cloud incidences for the YSUBL-RHx1.2, WUBL-RHx1.2, and COMP forecasts are significantly higher than the reference predictions and similar to the MODIS analysis, particularly in the WUBL-RHx1.2 and COMP simulations. The mean K_c indexes from the YSUBL-RHx1.2, WUBL-RHx1.2, and COMP forecasts are also more similar to the mean K_c obtained from observations compared to the reference simulations.

Table 3. Analogous to Table 1 for Aqua overpasses.

Cloud incidences at times of MODIS Aqua overpasses			
	All clouds	**Clouds tops > 3000m**	**Cloud tops < 3000m**
Reference forecasts	27.3	22.3	5.0
YSUBL-RHx1.2 forecasts	31.8	26.4	5.4
WUBL-RHx1.2 forecasts	37.2	28.5	8.7
COMP forecasts	39.1	29.1	10.0
MODIS analysis	39.1	28.3	10.8

Table 4. Analogous to Table 2 for Aqua overpasses.

K_c at times of Aqua overpasses			
	All clouds	**Clouds tops > 3000m**	**Cloud tops < 3000m**
K_c from reference forecasts	.71	.69	.80
K_c from YSUBL-RHx1.2 forecasts	.64	.60	.81
0 K_c from WUBL-RHx1.2 forecasts	.63	.58	.83
K_c from COMP forecasts	.62	.56	.80
K_c from measures	.58	.53	.70

In summary, the apparent underestimation of predicted cloud incidence compared with the MODIS data during the Terra satellite overpasses is consistent with the overestimation of predicted GHI in the late morning. Meanwhile, the apparent underestimation of predicted clouds and overestimation of the average clarity index at the times of the Aqua satellite overpasses is consistent with an overestimation of the GHI in the early afternoon, which is relatively higher than that in the late morning.

To gain insights into the differences in cloud incidence predictions obtained from the forecast systems considered, we plot their mean cloud incidences for each hour from 6:00 (around sunrise during NDJF) to 18:00. Figure 7 shows the cloud incidence frequency during NDJF for each hour from 8:00 to 18:00 based on the different forecasts for cloud tops higher than 3000 m (Fig. 7a), <3000 m (Fig. 7b), and lower than 1000 m (Fig. 7c)

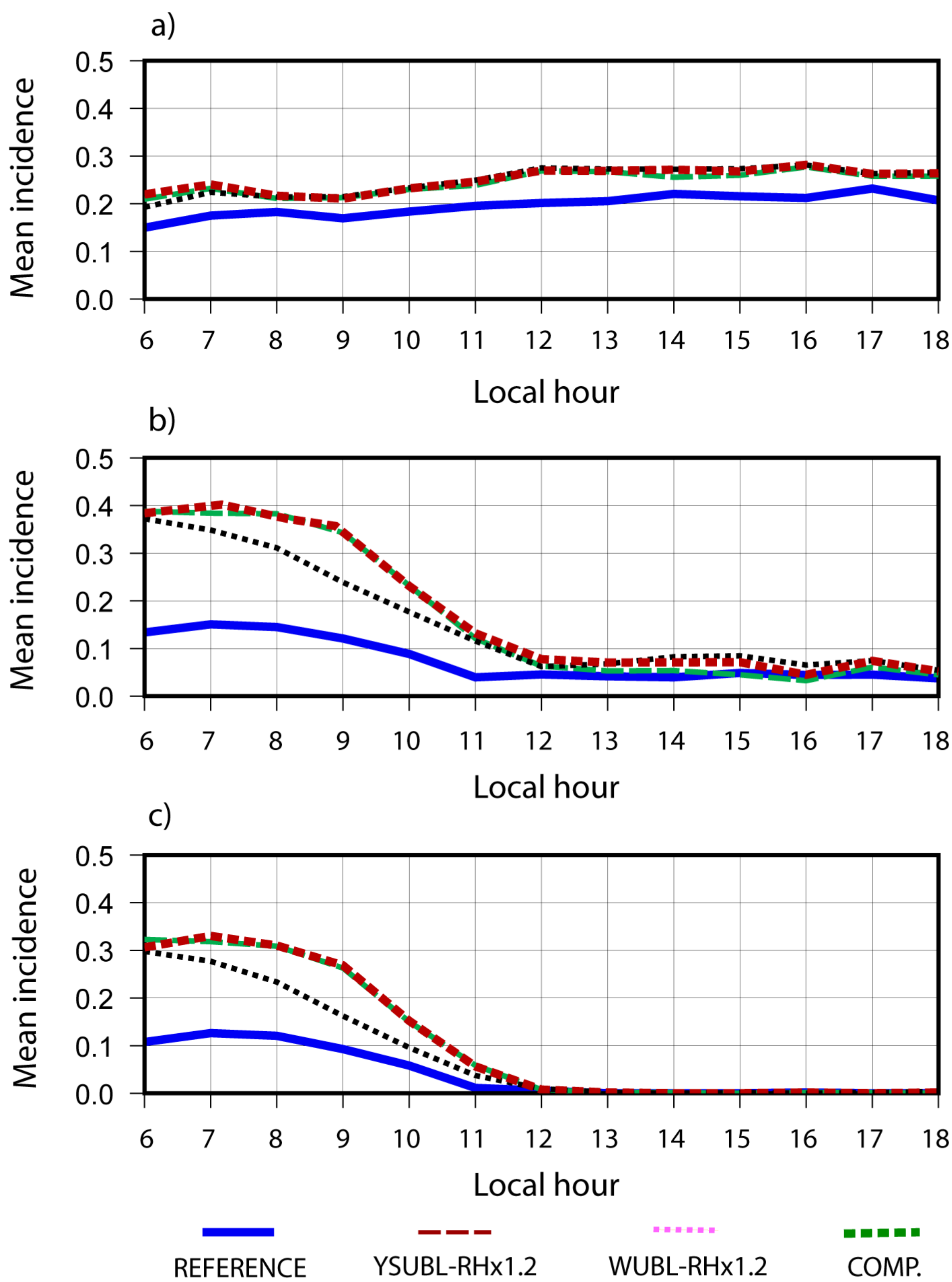

Figure 7. Forecasted cloud incidences during the NDJF season as a function of local time. Black, reference forecast; blue, YSUBL-RHx1.20 forecast; magenta, WUBL-RHx1.2 forecast; red, COMP forecast. (a) Clouds with tops >3000m. (b) Clouds with tops below 3000m. (c) Clouds with tops <1000m.

For high clouds, the YSUBL-RHx1.2, WUBL-RHx1.2, and COMP forecasts have similar incidences, which are higher than those in the reference forecasts. In all forecasts, there is a slight increase throughout the day. In contrast, low cloud cover shows a higher incidence in the morning for all forecasts. From 8:00 to 11:00, the YSUBL-RHx1.2, WUBL-RHx1.2, and COMP forecasts show a notable increase in incidence compared to the reference forecasts. Such an increase may not be realistic during the early morning hours (8:00–9:00), when the YSUBL-RHx1.2, WUBL-RHx1.2, and COMP forecasts show stronger negative GHI biases than those in the reference forecasts.

Between 10:00 and 12:00, the incidence of low clouds decreased across all forecasts. Compared to the MODIS analysis, the reference forecasts underestimate the low cloud incidence during this time, whereas the other forecasts slightly overestimate it. From

10:00 to 18:00, all forecasts show a relatively stable mean cloud incidence, with the YSUBL-RHx1.2, WUBL-RHx1.2, and COMP forecasts showing slightly higher incidences than the reference forecasts. In the early afternoon, the WUBL-RHx1.2 and COMP forecasts have average cloud incidences similar to the MODIS measurement based on the Aqua satellite data. There is also a significant reduction in positive biases in the reference simulation starting at 12:00.

A possible hypothesis regarding the performance of the reference predictions during this season is that the global predictions on which the regional simulations are based may have RH biases that depend on the level of the troposphere. The RH in the initial conditions may be realistic within the first 1000 m but not at higher levels, where it may have a negative RH bias. As the day progresses, ABL and shallow convection processes affect higher levels. The entire ABL becomes dryer since it mixes with relatively dry air, possibly contributing to underestimating low clouds after late morning. On the other hand, the possibility of overestimating surface heat fluxes can be another alternative hypothesis, also consistent with a progressive underestimation of low clouds. Fig. 10 shows the average ABL height and upward surface heat flux at Bonete for the reference simulations. The results for the other simulations are similar and are not presented here. The negative RH bias at the middle and higher tropospheres may contribute to the reference simulations' underestimation of clouds at these levels. Field measurement campaigns are necessary to verify the proposed hypothesis, as discussed in Section 4.

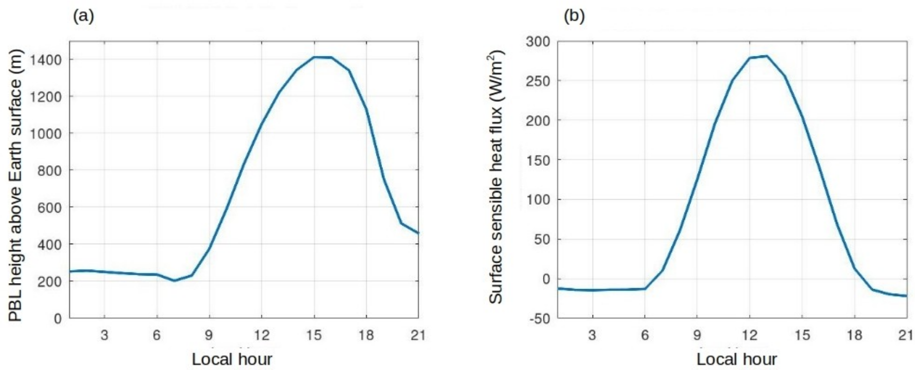

Figure 8. (a) Mean forecasted ABL height above the surface at Bonete during the NDJF season as a function of local time. (b) is analogous to (a) for forecasted upward heat flux from the surface.

Thus far, we have analyzed the biases in the GHI predictions, as well as the means of cloud incidence and K_c indices. As a measure of random errors, we include the RRMSE of the GHI predictions for each hour between 8:00 and 18:00 (Fig. 9). Between 8:00 and 10:00, the YSUBL-RHx1.2, WUBL-RHx1.2, and COMP forecasts exhibit higher errors than the reference forecasts. From 11:00 onward, the errors are similar. From 14:00 onward, the errors in the YSUBL-RHx1.2 and WUBL-RHx1.2 forecasts are lower than those in the reference forecasts.

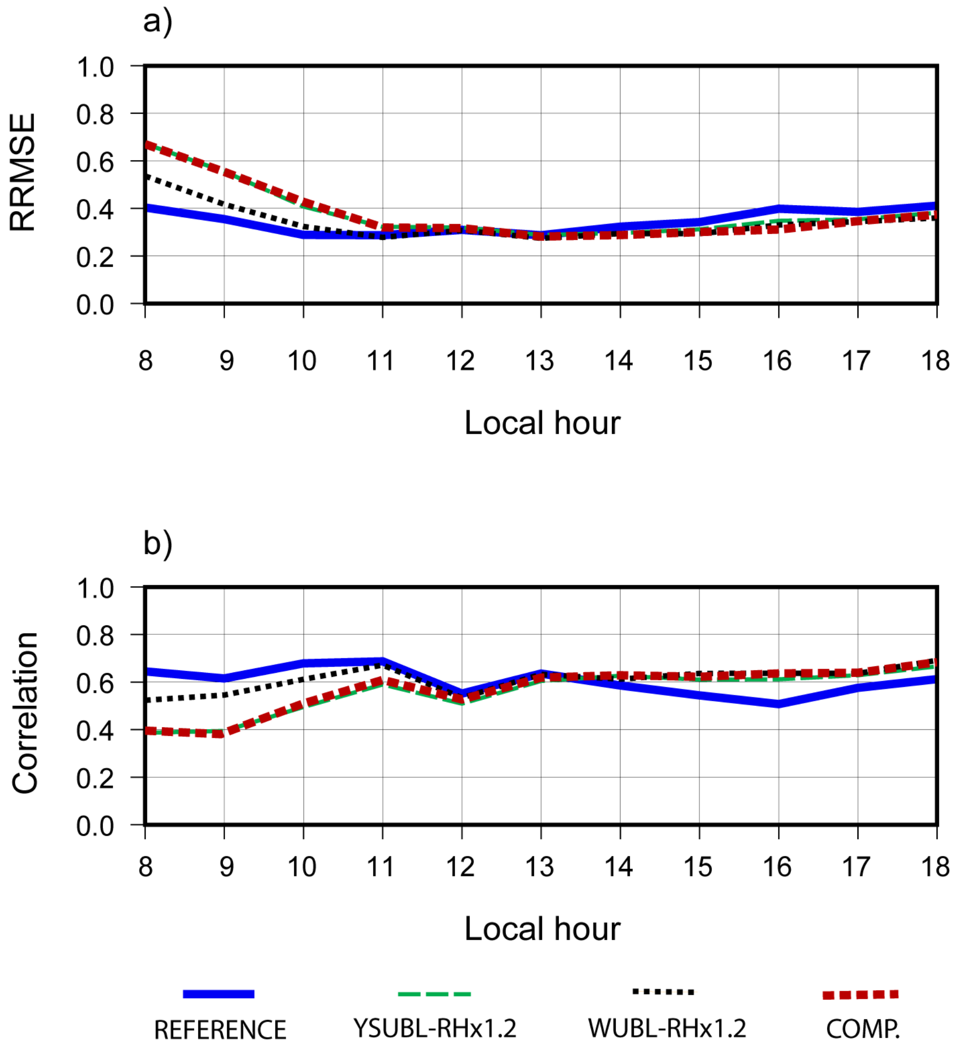

Figure 9. Relative RMSE of GHI forecasts at Bonete, during NDJF season, as a function of local time. Black, reference forecast, blue, YSUBL-RHx1.20; magenta, WUBL-RHx1.2, red, COMP forecast.

Fig. 10 shows the error distributions for clarity index predictions during the central hours of the day (11:00–17:00) for both the reference and COMP forecasts. The errors in the reference forecasts show a markedly asymmetrical distribution, which is consistent with the bias. In contrast, the errors in the COMP forecasts show a more symmetrical distribution, indicating an improvement. Therefore, the prediction performance of the alternative prediction systems is inferior to the reference simulation in the morning hours but exhibits less bias and more symmetrical error distributions after 12:00. This improvement is achieved with no corresponding increase in random errors during these hours.

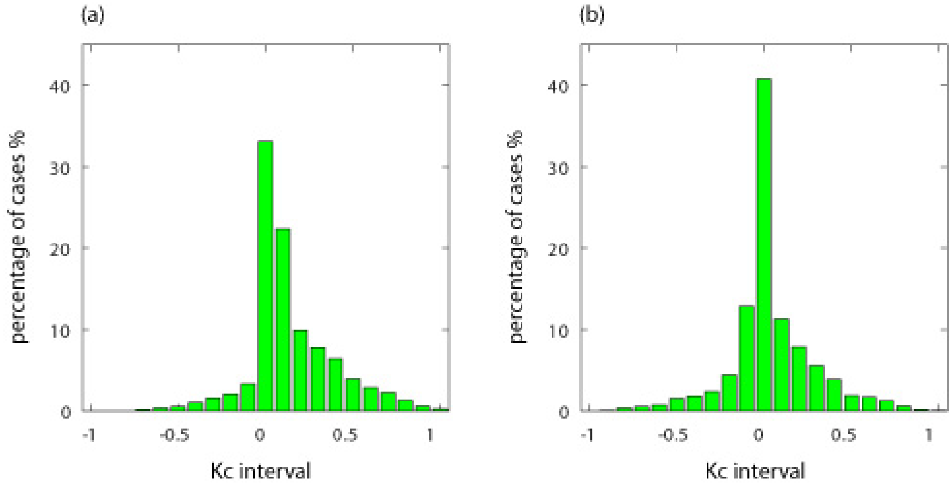

Figure 10. Histograms of forecast errors for the clarity index during NDJF, from 12:00 to 18:00 local time. (a) Reference forecasts. (b) COMP forecasts.

3.2. MJJA Season

Figure 11 shows the relative bias in the GHI reference predictions for the MJJA seasons between 2019 and 2023 for each hour between 9:00 and 16:00. Biases are negative throughout the day and significant from 9:00 to 12:00 and at 16:00. Moderate negative biases are observed during the central hours of the day (13:00 to 15:00).

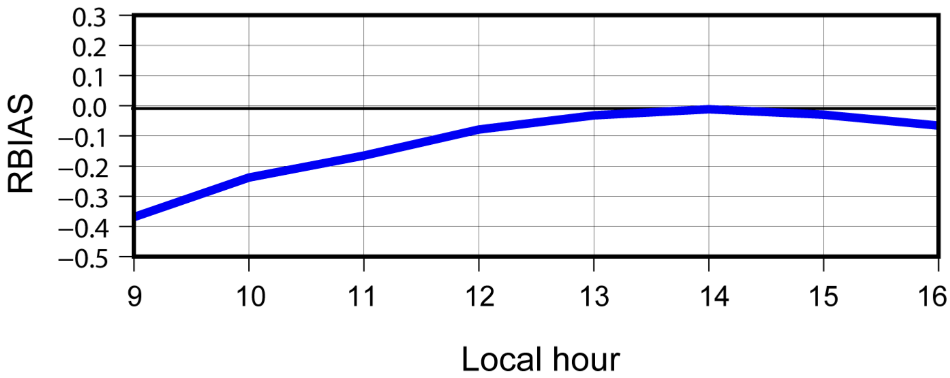

Figure 11. The relative bias of GHI from the reference forecasts at Bonete during the MJJA season.

Table 5 shows the cloud incidence forecast provided by the reference forecasts when the Terra satellite overpasses Bonete and the incidence diagnosed by the MODIS analysis. Table 6 shows the average K_c predicted by these simulations when predictions indicate cloud incidence during the Terra satellite overpass and the K_c obtained from GHI measurements in Bonete when the MODIS analysis detects clouds.

Table 5. Analogous to Table 1 for the MJJA season.

Cloud incidences at times of Terra overpasses			
	All clouds	**Clouds tops > 3000m**	**Cloud tops < 3000m**
Reference forecasts	47.2	25.4	21.8
MODIS Analysis	51.9	32.4	19.5

Table 6. Analogous to table 2, for MJJA season.

K_c at times of Terra overpasses			
	All clouds	**Clouds tops > 3000m**	**Cloud tops < 3000m**
K_c from reference forecasts	.35	.36	.34
K_c from measures	.54	.50	.60

Tables 7 and 8 are analogous to Tables 5 and 6 for the Aqua satellite overes. The reference simulations do not appear to overestimate cloud incidence (Tables 9 and 11), which does not contribute to explaining the underestimation of GHI in the predictions. However, such underestimation is consistent with the apparent underestimation of K_c shown in Table 10 and, to a lesser extent, in Table 12.

Table 7. Analogous to Table 10 for the Aqua satellite.

Cloud incidences at times of Aqua overpasses			
	All clouds	**Clouds tops > 3000m**	**Cloud tops < 3000m**
Reference forecasts	44.3	24.8	19.5
MODIS Analysis	54.2	36.0	18.2

Table 8. Analogous to Table 10 for the Aqua satellite

Mean K_c at times of Aqua overes			
	All clouds	**Clouds tops > 3000m**	**Cloud tops < 3000m**
K_c from reference forecasts	.41	.39	.43
K_c from measures	.53	.49	.59

To explore possible empirical corrections of the predictions, we compute K_c for each forecast of GHI at Bonete and deduce a new K_c index, K_c', as a convex linear combination between 1.0 and the original K_c.

$$K_c' = \alpha + (1 - \alpha)K_c \tag{8}$$

where α is a parameter between 0 and 1 to be set empirically. Note that $K_c < K_c' < 1$, $K_c' \rightarrow 1$ if $\alpha \rightarrow 1$ and $K_c' \rightarrow K_c$ if $\alpha \rightarrow 0$.

Then, the corrected forecast of GHI would be

$$corrected\, GHI\, fcst = (clear\, sky\, GHI).K_c' \tag{9}$$

To test this methodology, we select an alpha value of 0.2. The corrected forecasts show significant differences in bias at all hours. The absolute negative bias improves from 8:00 to 12:00 and decreases at 16:00. From 13:00 to 15:00, the corrected forecasts show a positive bias, with an absolute value larger than the original forecast. Figure 12b shows the RRMSE of the reference and corrected predictions. The corrected forecasts have a smaller RRMSE than the reference for all hours considered.

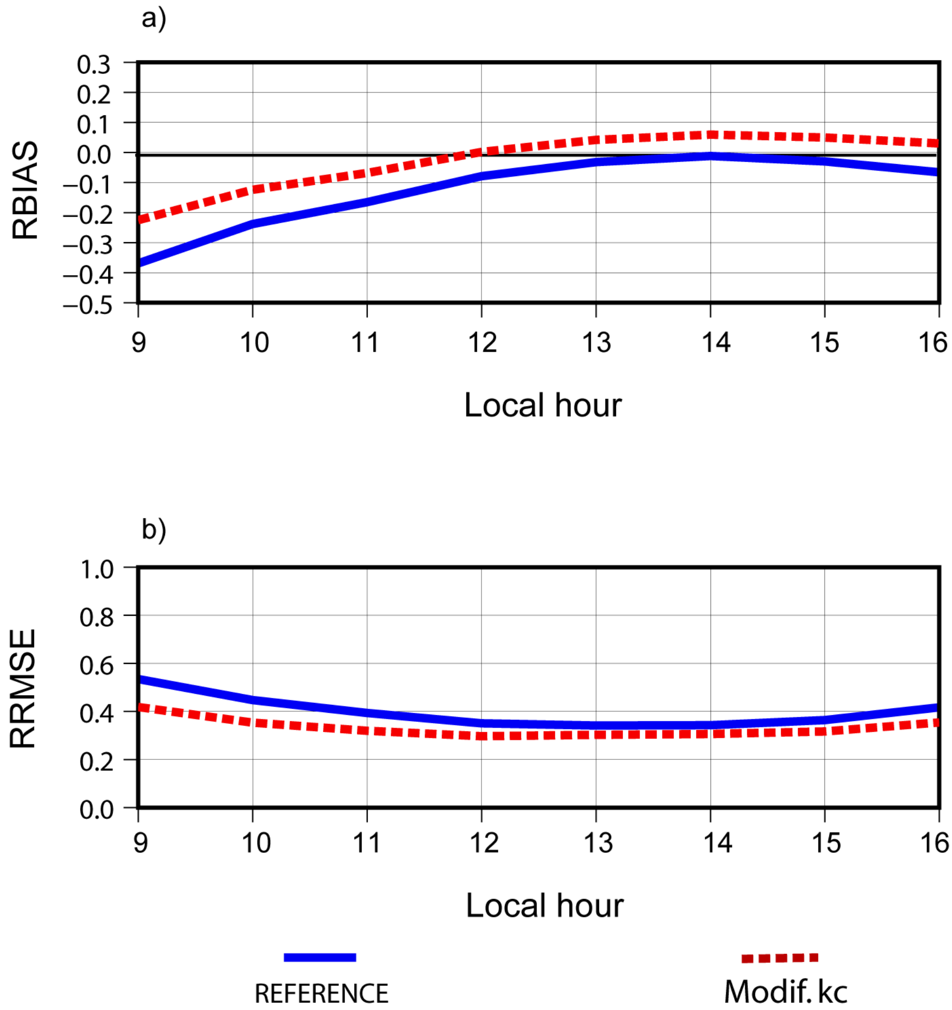

Figure 12. The relative bias of GHI from the reference forecasts at Bonete during the MJJA season.

To complement the field data of the Bonete station, we consider GHI estimates from NASA POWER analysis (referred to in Section 2) in two additional locations in Uruguay, located about 170km north and south of Bonete. The results are shown in Appendix B. The biases at these locations are consistent with those obtained from the Bonete station.

4. Conclusions

This study primarily evaluates a numerical system's performance in predicting GHI at a representative site in Uruguay, SESA, a humid subtropical region. The reference predictions have significant biases, with notable variations within the daily and annual cycles. This study also found significant biases in cloud incidence and clarity index predictions, with relevant diurnal and seasonal variations.

This work proposes methodologies that can improve the predictions; these are as follows:

- Modifications to the initial and boundary conditions of the numerical simulation;
- Post-processing of the simulation results.

Each of these methodologies has positive impacts on specific parts of the seasonal and diurnal cycles, and thus there is potential to combine them to optimize the forecast system's general performance. This work also proposes a hypothesis about the reasons for the prediction system's systematic errors.

Next, we present a summary of our findings.

In austral summer, the reference predictions underestimate GHI in the morning hours and overestimate GHI from 12:00 onward, with differences of about 10% in the observed mean GHI. When the Terra and Aqua satellites overpass the location of interest (late morning and early afternoon, respectively), the reference predictions underestimate the incidence of clouds, particularly for the Aqua satellite. We tested various parameterizations, including the WRF-Solar model, but the systematic deviations in the cloud incidence and GHI of the reference simulations remained. Adjusting the RH of the initial and boundary conditions by a factor of 1.20 has a significant impact. Although these simulations show worse bias in the morning hours compared to the reference, from 12:00 onward, there is a significant improvement in bias without an increase in the RRMSE, likely due to an increase in cloud incidence and, to a lesser extent, a decrease in K_c. We subsequently tested the performance of simulations involving two ABL schemes—YSU and WSU—and considered the lowest GHI prediction at Bonete for each hour. This combination produces moderate but statistically significant improvements in bias during the late afternoon. The histogram of errors of the COMP prediction is noticeably more symmetric than that of the reference simulation from 12:00 to 17:00. Moderate skewness is a desirable property for the practical use of a forecast system.

During austral winter, we observe a significant underestimation of GHI during much of the day, specifically from 8:00 to 10:00 and in the late afternoon. These biases are consistent with underestimating the mean K_c during the Terra and Aqua satellite overpasses. We employ a post-processing procedure in which K_c is recalculated, significantly improving relative bias. However, further research is needed to verify the role of this correction.

To complement the field data of the site used in this study, Bonete station, we considered GHI estimates from NASA POWER analysis in two additional locations in Uruguay, about 170 km north and south of Bonete. The biases at these locations are consistent with those obtained from the Bonete station (Appendix B).

5. Discussion

The current work is exploratory, and because GHI numerical predictions in SESA are so far scarcely documented, it is necessary. The findings can contribute to optimizing a GHI prediction system in the region, particularly the proposed techniques to alleviate biases. However, such optimization would imply actions beyond this work's scope.

In more detail, a fully operative forecast system requires putting into practice some actions additional to those described in this work:

- Optimizing the actions that were adequate to alleviate systematic errors—in particular, tuning the parameters that modified the initial and boundary conditions, or the kc index, depending on the time of the day and the time of the annual cycle.
- Using ensembles of forecasts based on global predictions with perturbed initial conditions. NOAA GFS produces ensembles of 30 such runs four times per day. Ensembles of several members require empirical adjustments of the forecast dispersion to make such dispersion a valuable measure of confidence intervals for the operative predictions or to express the forecast in probabilistic terms.
- Considering ensembles of forecasts based on global predictions of different origins.

Most of this study focuses on data from a pyranometer at a central Uruguay station and cloud diagnostics from MODIS analysis. To consider other locations within Uruguay and data from other sources, we use estimations of GHI from satellite measurements provided by the NASA POWER database. The results in these locations are consistent with those obtained with the GHI data from the station at Bonete, particularly the diurnal variation of the forecast's relative biases during the seasons selected to sample its annual cycle.

A possible hypothesis for the performance of the reference predictions during austral summer is that the global predictions on which the regional simulations are based may have RH biases that depend on the level of the troposphere. The RH in the initial conditions may be realistic within the first 1000 m but not at higher levels, where it may have a negative RH bias. This may reduce low-level clouds as the day progresses due to the relatively dry mix into the ABL. In addition, negative RH bias in the middle and higher tropospheres may contribute to the reference simulations' underestimation of clouts at these levels.

An alternative hypothesis is that the model underestimates the cloudiness due to parameterization errors. In this case, the RH modification may improve the predictions by compensating for errors. The initial conditions provided by the GFS system were compared with ERA analysis, finding very similar vertical profiles of temperature and specific humidity in the region of interest (these comparisons are not shown here). Consequently, future studies should consider conducting surveys of the vertical profile of the troposphere to a height of at least 5000 m during summer at various times of the day, which would be economically feasible using drones equipped with meteorological sensors. These data can then be combined with WRF models and nested large eddy simulations to understand the simulation dynamics better. These data can also be used to evaluate the performance of the radiosonde measurement network currently operational in the region and identify areas for improving measurements' frequency and geographic density to provide more accurate initial conditions for predicting atmospheric processes that impact GHI.

Funding: This research was funded by Agencia Nacional de Ivestigación e Inovación (ANII) of Uruguay, through the project FSE-1-2018-153056, NEFELE: predicción de Nubes para la generación de Energía Fotovoltaica Ensamblando modelación LES y de mesoescala", and by the Comisión Sectorial de Investigación Científica (CSIC) of the Universidad de la República of Uruguay, through the Régimen de Dedicación Total (RDT) program.

Data Availability Statement: Usinas y Trasmisiones del Estado (UTE) of Uruguay makes available data through its Sistema de Generación Eléctrica (SGE) site.

Acknowledgments: The field data used in this study were made available by Usinas y Trasmisiones del Estado (UTE) of Uruguay. The reviewers' comments significantly improved the manuscript.

Conflicts of Interest: The author declares no conflicts of interest.

MDPI	Multidisciplinary Digital Publishing Institute
DOAJ	Directory of open access journals
TLA	Three letter acronym
LD	Linear dichroism

Appendix A

Appendix A.1

The setting of the WRF model used in this work is similar to that of the work by Cazes Boezio and Ortelli (2019) [35]. The horizontal resolution is 0.25º. Figure 1 shows the grid points used to compute air temperature, pressure, density, and vertical velocity. The meridional and zonal components of wind are computed in points staggered by one-half of the horizontal resolution in the zonal and the meridional directions, respectively, according to the Arakawa C-grid. The vertical resolution considers 33 layers in the vertical direction. The model vertical coordinate is η, defined as

$$\eta = \frac{p_d - p_T}{p_S - p_T} \tag{A1}$$

where p_d is the hydrostatic component of dry air pressure at a particular atmosphere level and p_S and p_T are the analogous pressures at the Earth's surface and the atmosphere conventional top, respectively. The atmosphere top was set to 50 hPa. Table A1 gives the values of η at each layer interface.

Table A1. η values at the top of each layer of the vertical discretization.

Layer number	η at layer top	Layer number	η at layer top	Layer number	η at layer top
1	.987	12	.848	23	.709
2	.975	13	.836	24	.697
3	.961	14	.823	25	.684
4	.950	15	.811	26	.662
5	.937	16	.798	27	.624
6	.924	17	.785	28	.568
7	.912	18	.773	29	.494
8	.899	19	.760	30	.403
9	.886	20	.747	32	.295
10	.874	21	.735	32	.163
11	.861	22	.722	33	0.00

The horizontal velocities and the air temperature are computed inside each layer, while the vertical velocity is computed at the layer interfaces, according to the Lorenz vertical grid arrangement [1].

The parameterizations of physical processes used in this work are shown in Table A2.

Table A2. Parameterizarions of physical processes.

Physical Process	Scheme used
Short Wave Radiation	Dudia scheme [36]
Long Wave Radiation	RRTM scheme [37]
Surface Layer	Revised MM5 surface layer [38]
Atmospheric Boundary Layer	Yonsei University scheme [20]
Microphysics	Hong et al. scheme [39]
Cumulus Precipitation	Simplified Arakawa Schubert scheme [40]
Gravity Wave Drag	Kim Arakawa scheme [41]
Land Processes	Noah and surface model [42]

Figure A1 shows the procedure for producing initial and boundary conditions for the WRF simulations with the WPS module and the real.exe program. It also shows the procedure for modifying the total water content (RH variable) at the "met" files.

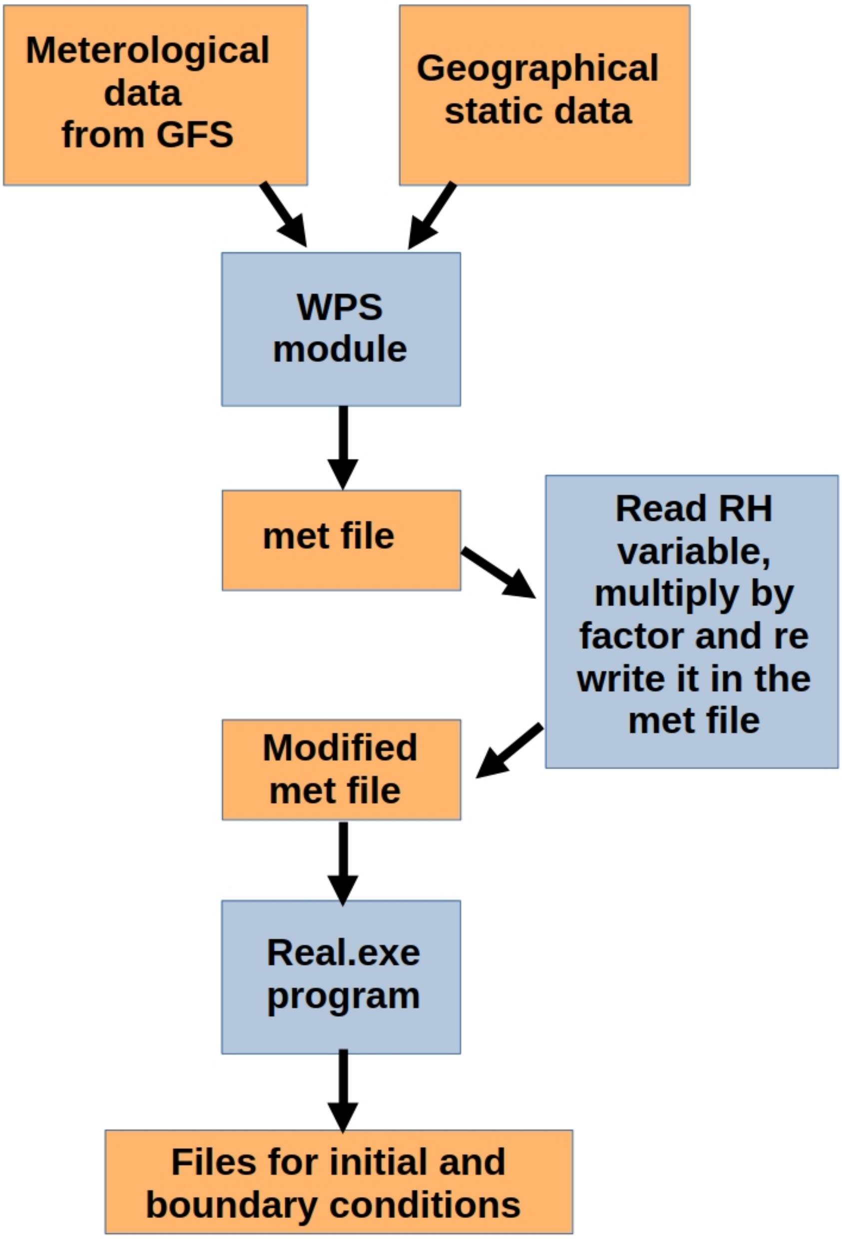

Figure A1. Scheme of the process to generate initial and boundary conditions with the WPS module and real.exe program and to modify the relative humidity variable of the "met" files.

Appendix B

Appendix B.1

In order to test the forecast results in contrast with data from the ground station at Bonete, we also used GHI estimations from the NASA POWER database. This database uses inter-res surface insolation values from satellite observations. The GHI measurements at Bonete were contrasted with the corresponding NASA power estimates. The mean GHI obtained from each source differs by less than 5%, and the correlation of hourly data is above 0.90 for most of the hours and months. In this Appendix, we show the relative bias of forecasted GHI compared to NASA POWER estimates for two other locations in Uruguay, at two points situated at the exact longitude of Bonete, one of them to the south of this site, close to the coast, and other to the North, in a more Mediterranean location. These points are named P South and P North, and their coordinates are 34.30ºS, 56.42ºW and 31.30ºS, 56.42ºW, respectively (see Fig. A2).

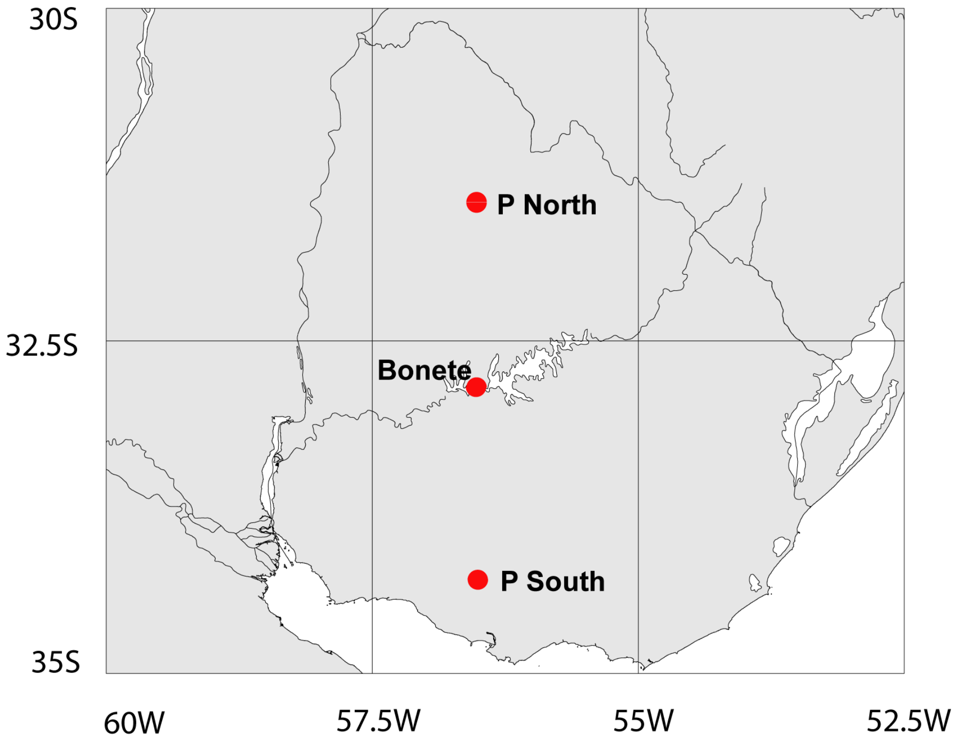

Figure A2. Location of P South and P North points.

Figure A3 shows the relative bias at these locations for the NDJF season as a function of local time (analogous to Fig. 5). It also shows the COMP forecast results. The biases of the reference forecast are very similar to those found in Bonete in Fig. 5; early morning forecasts underestimate the GHI from NASA POWER estimates, while during the central hours of the day and late afternoon, the predictions overestimate GHI from the analysis by 10% or more. As with the results in Bonete, the COMP forecasts worsen the underestimation of GHI during the early morning but improve the bias markedly during the central hours and late afternoon. The results of COMP forecasts reduced RRMSE slightly during the central hours of the day and the afternoon (this is not shown here).

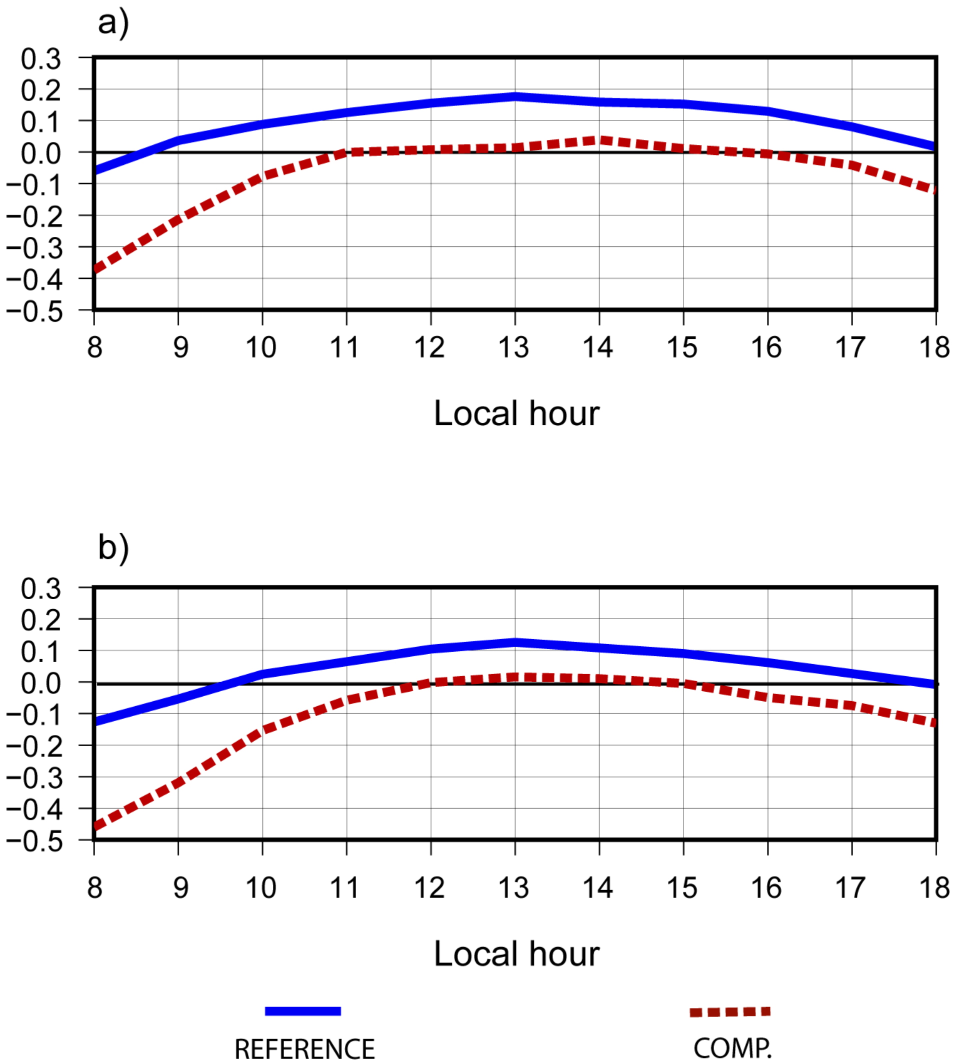

Figure A3. a) The relative bias of GHI from the reference forecasts during the NDJF season (continuous blue line) and from the COMP forecasts (dashed red line) with respect to NASA POWER data at the P South location. b) is analogous to a) for the P North location.

During MJJA (Fig A4), the results showed a substantial underestimation during the morning hours, similar to that for the Bonete station, and to a lesser extent during late afternoon. The empirical corrections of the Kc index from the model output improved the bias significantly without worsening the RRMSE during the morning hours (this is not shown here).

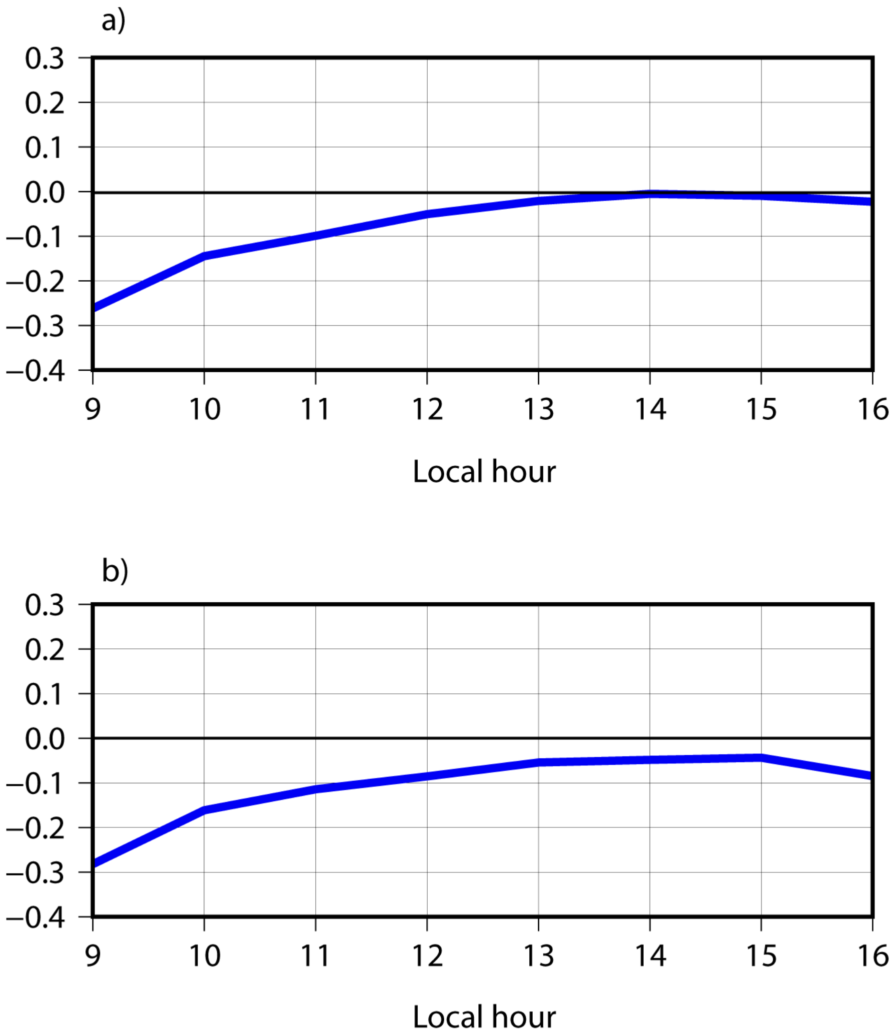

Figure A4. a) The relative bias of GHI from the reference forecasts with respect to NASA POWER data at the P South location. b) is analogous to a) for the P North location.

In conclusion, the data from NASA POWER and Bonete station validate each other reciprocally, and the results obtained at Bonete apply to wider regions of Uruguay.

References

1. Mathiesen P.; Kleissl J. Evaluation of numerical weather prediction for intra-day solar forecasting in the continental United States Deparhttps://doi.org/10.1016/j.renene.2024.121361A New Look into the South America Precipitation Regimes: Observation and Forecast. *Solar Energy* **2011**, *85*, 967-977. doi:10.1016/j.solener.2011.02.013
2. Huang J.; Thatcher M. Assessing the value of simulated regional weather variability in solar forecasting using numerical weather prediction. *Solar Energy* **2017**, *144*, 529-539. http://dx.doi.org/10.1016/j.solener.2017.01.058
3. Bezerra Amorim A. C.; de Almeida Dantas V.; Souza dos Reis J.; de Assis Bose N.; de Azevedo Santos S.; Vaca E.; Cruz Bezerra L. A.; Alves de Matos M. F.; Torres Correia de Mello Nobre M.; de Lima Oliveira L.; de Medeiros A. M. Analysis of WRF-solar in the estimation of global horizontal irradiation in Amapá, northern Brazil *Renewable Energy* **2024**, *235*, 121361. https://doi.org/10.1016/j.renene.2024.121361
4. Rincón A.; Jorbab O.; Frutosa M.; Alvarez l.; Barriosa F. P.; Gonzáleza J. A. Bias correction of global irradiance modelled with weather and research forecasting model over Paraguay. *Solar Energy* **2017**, *170*, 201-211 https://doi.org/10.1016/j.solener.2018.05.061
5. Texeira Branco V.; Alonso R.; Cazes Boezio G. Pronóstico del día siguiente de la Radiación Solar en la región de la Pampa Húmeda. *Revista Brasileira de energia Solar* **2022**, *13*, 11-19 https://doi.org/10.59627/rbens.2022v13i1.377
6. Ferreira, G. W.; Reboita M. S. A New Look into the South America Precipitation Regimes: Observation and Forecast. *Atmopshere* **1978**, *13*, 873, pp 33.
7. Gan M.; Rao V. B. Surface Cyclogenesis over South America. *Mon. Wea. Rev.* **1991**, *119*, 1293–1302.
8. Rao V. B.; Do Carmo A. M. C.; Franchito S. H. Seasonal variations in the southern storm tracks and associated wave propagation. *J. Atmos. Sci.* **2002**, *59*, 1029-1040.

9. Vera C.; Vigliarolo P. K.; Berbery E. H. Cold season synoptic–scale waves over subtropical South America. *Mon. Wea. Rev.* **2002**, *130*, 684-699.
10. Ross, B. B.,; Orlanski, I. The Circulation Associated with a Cold Front. Part II: Moist Case. *J. A. S.* **1978**, *35*, 445-465. https://doi.org/10.1175/1520-0469(1978)035<0445:TCAWAC>2.0.CO;2
11. Rasmussen, K. L.; Chaplin, M. M.; Zuluaga, M. D.; Houze, R. A. Contribution of extreme convective storms to rainfall in South America. *J. Hydrometeorol.* **2016**, *17*, 353–367.
12. Siqueira, J. R.; Machado L. A. T. Influence of the frontal systems on the day-to-day convection variability over South America. *J. Climate* **2004**, *10*, 1754–1766.
13. Velasco, I.; Fritsch J. M. Mesoscale convective complexes in the Americas. *J. Geophys. Res.* **1987**, *10*, 9591–9613. https://doi.org/10.1029/JD092iD08p09591
14. Salio, P.; Nicolini, M.; Zipser, E.J. Mesoscale convective systems over southeastern South America and their relationship with the South American low-level jet. *JMon. Weather Rev.* **2007**, *135*, 1290–1309.
15. Seluschi M. E.; Saulo A. C. Possible mechanisms yielding an explosive coastal cyclogenesis over South America: experiments using a limited area model. *Aust. Met. Mag.* **47**, *47*, 309–320.
16. Satyamurty P.; Bittencourt D. P. Performance evaluation statistics applied to derived fields of NWP model forecasts. *Weather Forecast* **1999**, *14*, 726–740.
17. Orteli, S. O. Avances en predicciones meteorológicas para la gestión de sistemas hidroeléctricos : Un análisis comparativo entre ECMWF y GFS en el Río Negro, Uruguay. Mg. Sci. Thesis, Universidad de la República, Uruguay, 2023. Available at https://www.colibri.udelar.edu.uy/jspui/handle/20.500.12008/41905
18. Porrini, C. Evaluación del modelo regional WRF para pronósticos de radiación solar en superficie dentro del territorio uruguayo. MB Thesis, Universidad de la República, Uruguay, **2017**, Available at https://www.colibri.udelar.edu.uy/jspui/handle/20.500.12008/19177
19. Skamarock, W. C.; Klemp, J. P.; Dudhia, J.; Gill, D. G.; Liu, Z.; Berner, J.; Wang, W.; Powers, J. G.; Duda, M. G.; Marker, D. M.; Huang, X. Y. A Description of the Advanced Research WRF Model Version 4. Technical Report, Nacional Center of Atmospheric Research (NCAR), USA, **2017**. Available at https://n2t.org/ark:/85065/d72r3vrp
20. Hong, S. Y.; Noh Y. Dudhia J. A new vertical diffusion package with an explicit treatment of entrainment processes. *Mon. Wea. Rev.* **2006**, *134*, 2318–2341. doi:10.1175/Mwr3199.1.
21. Bretherton, J. R. McCaa J. R., Grenier H. 2004: A New Parameterization for Shallow Cumulus Convection and Its Application to Marine Subtropical Cloud-Topped Boundary Layers. Part I: Description and 1D Results. *Mont. Wea. Rev.* **2004**, *132*, 864–882.
22. Konor, C. S.; Cazes Boezio G.; Mechoso, C. R.; Arakawa A. Parameterization of ABL Processes in an Atmospheric General Circulation Model: Description and Preliminary Assessment. *Mon. Wea. Rev.* **2009**, *137*, 1061–1063.
23. Lock, A. P. The parameterization of entrainment in cloudy boundary layers. *Quart. J. Roy. Meteor. Soc.* **1998**, *124*, 2729–2753.
24. Park S.; Bretherton C. S. The University of Washington Shallow Convection and Moist Turbulence Schemes and Their Impact on Climate Simulations with the Community Atmosphere Model.*Jour. of Climate* **2009**, *22*, 3449–3469.
25. Grell, G.A. Prognostic evaluatION of assumptions used by cumulus Parameterizations.*Mont. Wea. Rev.* **1993**, *121*, 764–787.
26. Kain, J. S.; Fritsch, J. M. Convective Parameterization for Mesoscale Models: The Kain-Fritsch Scheme. In *The representation of cumulus convection in numerical models*; Emanuel, K.A. and Raymond, D.J., Eds., Springer, Berlin, 165-170. https://doi.org/10.1007/978-1-935704-13-3_16
27. Cornalino E.; Draper M. Author 1, A.B.; Author 2, C.D.; Author 3, E.F. Planning the Distribution of Wind Farms in Uruguay in Order to Optimize the Operability of Large Amounts of Wind Power. In Proceedings of the 2012 European Wind Energy Conference (2012 EWEC), Copenhagen, Denmark , 2012. Available online: www.fing.edu.uy/cluster/eolica/publi/ Cornalino_Draper_EWEC2012_FINAL.pdf
28. Platnick S.; King M. D.; Meyer K. G.; Wind G.; Amarasinghe N.; Marchant B. Arnold G. T.; Zhang Z.; Hubanks P. A.; Ridgway B.; Riedi J. MODIS Cloud Optical Properties: User Guide for the Collection 6 Level-2 MOD06/MYD06 Product and Associated Level-3 Datasets. NASA Goddard Space Flight Center. Available online: https://MODIS-images.gsfc.nasa.gov/_docs/C6MOD06OPUserGuide.pdf
29. King, M. D.; Menzel W. P.; Kaufman, Y. J.; Tanré D.; Gao B. C.; Platnick S.; Ackerman S.; Remeret L.; Pincus R.; Hubanksal, P. A. Cloud and aerosol properties, precipitable water, and profiles of temperature and water vapor from MODIS. *EEE Transactions on Geoscience and Remote Sensing* **2003**, *41*, 442–458. DOI: 10.1109/TGRS.2002.808226
30. Platnick, S.; Meyer, K.; Wind, G.; Holz, R. E.; Amarasinghe, N.; Hubanks, P. A.; Marchant, B.; Dutcher, S.; Veglio, P. The NASA MODIS-VIIRS Continuity Cloud Optical Properties Products. *Remote Sens.* **2021**, *13(1)*, https://doi.org/10.3390/rs13010002
31. Lauret, P., et al. NASA POWER Database: Long-Term Solar and Meteorological Data for the Renewable Energy Community. *IEEE Transactions on Sustainable Energy* **2017**, *8*, 1115-1123. DOI: 10.1109/TSTE.2016.2622499
32. Platnick, S.; Meyer, K.; Wind, G.; Holz, R. E.; Amarasinghe, N.; Hubanks, P. A.; Marchant, B.; Dutcher, S.; Veglio, P. The NASA MODIS-VIIRS Continuity Cloud Optical Properties Products. *Remote Sens.* **2021**, *13(1)*, https://doi.org/10.3390/rs13010002
33. Press W. H.; Teukolsky S .A.; Vetterling W. T.; Flannery P. B. *Numerical Recipes in Fortran 77*, 2nd ed.; Publisher: Cambridge University Press, Publisher Location, Cambridge, United Kindom, 1992; pp. 609–613.

34. Snedecor G. W.; Cochran W. G.. *Métodos Estasdísticos*, 3rd ed.; Publisher: CECSA, Mexico DF, Mexico, 1979; pp. 270–278.
35. Cazes Boezio, G.; Orteli, S. Use of the WRF-DA 3D-Var Data Assimilation System to Obtain Wind Speed Estimates in Regular Grids from Measurements at Wind Farms in Uruguay. *Data* **2019**, *4(4), 142* https://doi.org/10.3390/data4040142
36. Dudhia, J. Numerical study of convection observed during the winter monsoon experiment using a mesoscale two-dimensional model. *J. Atmos. Sci.* **1989**, *46*, 307–310.
37. Iacono, M.J.; Mlawer, E.J.; Clough, S.A.; and coauthors. Impact of an improved longwave radiation model, RRTM, on the energy budget and thermodynamic properties of the NCAR community climate model, CCM3. *J. Geophys. Res. Atmos.* **2000**, *105 (D11)*, 14873–14890.
38. Jimenez, P.; Dudhia, J.; Gonzalez-Ruoco, J.F.; Navarro, J.; Montavez, J.P.; Garcia-Bustamente, F. A revised scheme for the WRF surface layer formulation. *Mon. Weather Rev.* **2012**, *140*, 898–918.
39. Hong, S.Y.; Dudhia, J.; Chen, S.H. A Revised Approach to Ice Microphysical Processes for the Bulk Parameterization of Clouds and Precipitation. *Mon. Weather Rev.* **2004**, *132*, 103–120.
40. Grell, G.A. Prognostic evaluation of assumptions used by cumulus parameterizations. *Mon. Weather Rev.* **1993**, *121*, 764–787.
41. Kim, Y.J.; Arakawa, A. Improvement of Orographic Gravity Wave Parameterization Using a Mesoscale Gravity Wave Model. *J. Atmos. Sci.* **1995**, *52*, 1875–1902.
42. Niu, G.-Y.; Yang, Z.L.; Mitchel, K.E.; Chen, F.; Ek, M.B.; Barlage, M.; Kumar, A.; Manning, K.; Niogi, D.; Rosero, E. The community Noah land surface model with multiparameterization options (Noah-MP): 1. Model description and evaluation with local-scale measurements. *J. Geophys. Res.* **2011**, *116 (D12)* https://doi.org/10.1029/2010JD015139